

On the equilibrium profiles of asymmetric sand ripples under nonlinear shoaling waves

F.Y. Testik¹, S.I. Voropayev^{1,2}, S. Balasubramanian¹, and H.J.S. Fernando¹

¹Department of Mechanical and Aerospace Engineering, Arizona State University,
Tempe, AZ, 85287-9809

²Institute of Oceanology, Russian Academy of Sciences, Moscow, 117851, Russia

Results of laboratory experiments conducted to study the equilibrium profiles of asymmetric sand ripples that form under nonlinear shoaling waves are reported. Waves were generated in a large wave tank with a sandy slope that models the oceanic coastal zone. Detailed profile data on asymmetric sand ripples that form under such conditions were collected and their analysis revealed that to the first approximation the equilibrium profiles can be considered as self-similar. In the experimental parameter range considered, ripple profiles could be satisfactorily modeled by a simple “universal” dimensionless profile of “saw tooth” shape. The results have applications to shallow water acoustic problem involving the detection of buried objects in the ocean bottom using low frequency Sonar’s.

Index terms: 4217, 4203, 4460, 4558

Keywords: sand ripples; shoaling waves, equilibrium ripple profile

Corresponding author

S.I. Voropayev

Tel: (480) 965-3770

Fax: (480) 965-8746

E-mail: s.voropayev@asu.edu

1. Introduction

Sand ripples are relatively small-scale wavy sand structures that form under the action of wave forcing in the coastal regions and laboratory (Figures. 1a,b). These structures are frequently (quasi-) two-dimensional, regular and are oriented parallel to the wave front. The generic mechanism of their formation is instability at the sand-water interface, which arises when the near bottom water velocity exceeds a critical value. Since the pioneering study by *Darwin* [1883], sand ripples have been of considerable interest due to their vivid coastal engineering applications [e.g., *Sleath*, 1984; *Nielsen*, 1992]. Nonlinear processes involved in the formation and dynamics of ripples, however have been not well understood, and on the theoretical front even the weakly non-linear analysis has been conducted only recently [*Blondeaux*, 1990; *Vittory and Blondeaux*, 1990; *Andersen*, 2001]. Numerical analysis is also notably difficult due to the particular complications associated with mathematically representing the sand-water interaction problems, such as modeling sediment transport and changing boundaries [*Summer et al.*, 2003]. The advent of high-resolution multi beam sonar with resolution down to 5-10 cm has enabled detailed coastal observations, however, the high resolution coastal scanning has limited practical utility in ripple evolution studies [*Mayer et al.*, 2002]. Therefore, experimental modeling remains one of the most effective methods to study ripples. In the experiments the background flow is usually symmetric and the resulting ripples are also symmetric [*Sleath*, 1984; *Nielsen*, 1992; *Faraci and Foti*, 2001; *Hansen et al.*, 2001; *Scherer et al.*, 1999]. Growing naval applications of detecting solid bottom objects such as buried mines using acoustic techniques [*Richardson et al.*, 2001; *Chotiros*, 1995) have necessitated a better knowledge of the equilibrium ripple profiles, especially for the case of asymmetric background flow where asymmetric ripples (see Figures 1c,d) are formed. The experimental data on such ripples (ripples formation, equilibrium sizes and drift) are reported

in *Voropayev et al.*, [2003] and below we concentrate mostly on their equilibrium profiles that has not been considered previously.

2. Experimental set-up and flow conditions

A detailed description of the experimental facility is given in *Voropayev et al.* [2003a,b], and only a brief description is given below. The oceanic coastal zone was modeled in a wave tank (32 x 0.9 x 1.8 m) with a slopping (slope angle, $\beta = 2.5^\circ$) sandy bottom (mean grain size, $d_{50} = 0.04$ cm, thickness 20 cm). The vertical paddle, driven by a piston, is used to generate sinusoidal periodic waves in the water of the depth 100 cm near the paddle. In three experiments the frequency, ω , and peak-to-peak horizontal displacements of the paddle, $2\varepsilon_0$, were $\omega = 0.4$ Hz and $2\varepsilon_0 = 15, 20$ and 25 cm, respectively, and in one experiment $\omega = 0.2$ Hz and $2\varepsilon_0 = 20$ cm were used. The tank consists of a number of sections (61 cm in length) with section 0 near the paddle and below the positions along the slope is given as section numbers. Although the wave paddle forcing is sinusoidal, when the waves propagate along the slope, they steepen and change their height as in the nature, thus causing the underlying velocity field to become increasingly nonlinear and asymmetric (see Figure 3). Before each experiment the sand on the slope was made flat. The waves were then initiated and sand ripples started forming along the slope. When the ripples reach their equilibrium state, information on their characteristics was collected from video records and quantitative data were obtained by using the so-called “structured light” method with the accuracy ± 0.1 cm [Faraci et al., 2000]. In this method, a narrow vertical laser sheet is used to produce a bright line along the tank axis at the bottom. This line is straight if the bottom is flat or curved if the bottom is undulated with the curvature being directly related to the sand surface elevation. Using a high-resolution digital camera, this line was photographed periodically (Figure 1d) through the glass sidewalls, and using commercial software (TSI-Insight) the images of the

line were transformed into the sand surface elevations using scaling factors for horizontal and vertical coordinates.

3. Experimental results

A total of four experimental runs with different wave forcing were conducted. However, since the characteristics of shoaling waves change as they propagate along the slope, ripples forming at different sections of the tank have different characteristics. Therefore, each experimental run provides a number of ripple profiles corresponding to varying wave conditions along the slope. Below, first we present quantitative experimental data on the equilibrium ripple characteristics and then describe an effort to parameterize equilibrium ripple profiles.

In Figure 4 we give the measured values of equilibrium ripple length, L (horizontal distance between two nearest troughs), and height, h (vertical distance from the crest to the offshore trough), along the slope for different experimental runs. In this figure d gives the distance along the slope from the wave paddle. As can be seen, the ripple size (both L and h) increases along the slope in the onshore direction (increasing d) due to the increase in the local horizontal water particle excursion, 2ε , as the waves shoaling along the slope. The data shown in Figure 4 are instantaneous (not averaged) and the data scatter can be explained by the long-term ripple instability [Voropayev *et al.*, 1999], which results to periodic splitting and merging of the ripples, and hence values of the ripple characteristics fluctuate around their equilibrium values.

Due to the waves asymmetry (Figure 3), ripples forming under those waves are also asymmetric (Figures 1c,d). In Figure 5, typical sand surface elevations as measured at different sections along the slope are given for the experimental run $\omega = 0.4$ Hz, $2\varepsilon_0 = 15$ cm. As can be seen, all ripples along the slope are asymmetric with ripple crests positioned closer

to their onshore troughs, thus leading to steeper onshore sides of ripples. Also note that larger ripples form in sections closer to the shore.

Although the ripple size changes significantly along the slope, equilibrium profiles of these asymmetric ripples show a marked similarity in shape. To enhance this similarity, the ripple profiles, taken in different sections, were plotted together in one graph and are shown in Figures 6a-d for each experimental condition. For clarity, only selected profiles are given and the inset in Figure 6a explains the coordinate system.

The data of Figures 6a-d suggest that ripple profiles at different flow conditions can be approximated by some “universal” profile. In order to quantify such a profile, we consider, as a first step, a “saw tooth” shape profile shown in the inset in Figure 7. In this schematic the imaginary line, which is parallel to the tank bottom and connects the offshore and onshore troughs of the ripple represents the bottom side of the triangle and two lines that give the best fit to the onshore and offshore sides of the ripple represent the corresponding sides of the triangle. Onshore and offshore sides of the triangle make angles θ_1 and θ_2 with the bottom side, respectively. The measured values of θ_1 and θ_2 for ripples formed along the slope in different experimental runs are given in Figure 7. In this figure, the symbols around the upper dashed line represent experimental data for θ_1 , while symbols around the lower dashed line represent the data for θ_2 and the dashed lines show the best fits to these data. As can be seen in this figure, although θ_1 and θ_2 have some scatter, their mean values are approximately constant and equal to $\theta_1 = 35^\circ$ and $\theta_2 = 19^\circ$ for different ripples formed along the slope for the range of our experimental conditions. Note that when the slope of the tank bottom, $\beta = 2.5^\circ$, is taken into account, the value of the “avalanche” angle (angle of repose), ϕ , for the particular sand used in our experiments ($\phi \approx 32^\circ$; see *Sleath*, 1984) becomes approximately equal to the value of θ_1 . However, the physical sense of θ_2 remains an open question.

The experimental fact that θ_1 and θ_2 are approximately constants permits us to introduce a simple “universal” dimensionless ripple profile where horizontal, x , and vertical, z , coordinates of the observed ripples are scaled with their equilibrium lengths, L , and heights, h , respectively. From simple geometrical considerations one arrives at the following parameterization

$$z^* = \begin{cases} C^{-1} [x^* \tan(\theta_1 - \beta) + \sin \beta], & 0 \leq x^* \leq C / \tan \theta_1 \\ C^{-1} (1 - x^*) \tan(\theta_2 + \beta), & C / \tan \theta_1 < x^* \leq 1 \end{cases}, \quad (1)$$

where $z^* = z/h$, $x^* = x/L$ and $C = h/L = \tan \theta_1 \tan \theta_2 / (\tan \theta_1 + \tan \theta_2) \approx 0.23$ is the averaged ripple steepness. Note that this empirical steepness falls in the range of steepness values ($0.15 < h/L < 0.25$) reported in *Sleath* [1984] for the general class of vortex ripples, either symmetric or asymmetric. In Figures 8a-d, all dimensionless ripple profiles measured in different sections along the slope for different experimental runs are shown by symbols, and proposed parameterization (1) is shown by solid lines. The general agreement is satisfactory, except perhaps in the close vicinity of the ripple crests and troughs.

4. Conclusions

It is well known that the ocean bottom responds to linear symmetric waves by forming symmetric ripples. Under shoaling waves the forcing is asymmetric and the ripples are also asymmetric. In our experiments shoaling waves were generated in a large wave tank with a sandy slope that models the oceanic coastal zone. Since the characteristics of shoaling waves change as they propagate along the slope, ripples forming at different locations of the tank also have different characteristics. Therefore, each experimental run provided information on a large number of ripple profiles associated with different wave conditions. The analysis of the experimental data show that to the first approximation the equilibrium profiles of asymmetric ripples may be considered as self-similar. Simple saw tooth type “universal” similarity profile was found to fit the experimental data reasonably well. The results is

expected to have useful applications in shallow water acoustics, where propagation and scattering of low frequency ($\sim 10\text{Khz}$) acoustic by ripples is one of the important aspects for the detection of buried objects in the ocean floor.

Acknowledgments. This research was supported by the Office of Naval Research, Grant N-00014-01-1-0349.

References

- Andersen K.H. (2001), A particle model of rolling grain ripples under waves, *Phys. Fluids*, *13(1)*, 58.
- Blondeaux P. (1990), Sand ripples under sea waves. Part 1. Ripple formation, *J. Fluid Mech.*, *218*, 1.
- Chotiros, N.P. (1995), Biot model of sound propagation in water-saturated sand, *J. Acoustic Soc. America*, *97*, 199.
- Darwin G.H. (1883), On the formation of ripple-mark in sand, *Proc. R. Soc. London*, *36*, 18.
- Faraci C. and Foti E. (2001), Evolution of small scale regular patterns generated by waves propagating over a sandy bottom, *Phys. Fluids*, *13(6)* 1624.
- Faraci C., Foti E. and Baglio S., (2000), Measurements of sandy bed scour processes in an oscillating flow by using structured light. *Measurement*, *28*, 159.
- Hansen J.L., Hecke M.V., Haaning A., Ellegaard C., Andersen K.H., Bohr T. and Sams T. (2001), Pattern formation: instability in sand ripples, *Nature*, *410*, 324.
- Mayer L.A. and Baldwin K.C. (2002), Shallow water surveys, 2001: High resolution surveys in shallow water, *Marine Technology Society*, *35(4)*, 3,.
- Nielsen P. (1992), *Coastal Bottom Boundary Layers and Sediment Transport*, World Scientific.
- Richardson, M.D.; Briggs, K.B.; Bibee, L.D.; Jumars, P.A. et al.; (2001), Overview of SAX99: Environmental considerations, *IEEE Journal Ocean Eng.*, *26(1)*, 26.
- Scherer M.A., Melo F. and Marder M. (1999), Sand ripples in an oscillating annular sand-water cell, *Phys. Fluids*, *11(1)*, 58.
- Sleath J.F.A. (1984),. *Sea Bed Mechanics*, Wiley.
- Summer B.M., Chua L.H.C., Cheng N.S. and Fredsoe J. (2003), Influence of turbulence on bed load sediment transport, *J. Hydraulic Eng., ASCE*, *129(8)*, 585.

- Vittory G. and Blondeaux P. (1990), Sand ripples under sea waves. Part 2. Finite-amplitude development, *J. Fluid Mech.*, 218, 19.
- Voropayev S.I., McEachern G.B., Boyer D.L. and Fernando H.J.S. (1999), Dynamics of sand ripples and burial/scouring of cobbles in oscillatory flow, *Appl. Ocean Res.*, 21(5), 249.
- Voropayev S.I., Testik F.Y., Fernando H.J.S. and Boyer D.L. (2003a), Burial and scour around short cylinder under progressive shoaling waves, *Ocean Eng.*, 30(13), 1647.
- Voropayev S.I., Testik F.Y., Fernando H.J.S. and Boyer D.L. (2003b), Morphodynamics and cobbles behavior in and near the surf zone, *Ocean Eng.*, 30(14), 1741.

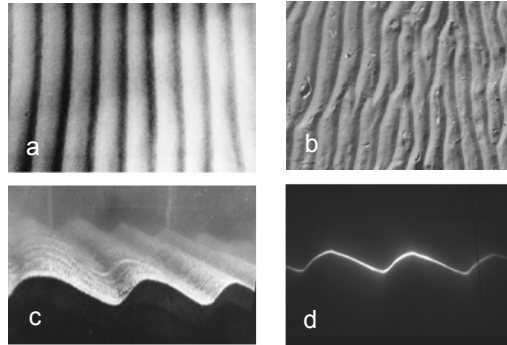


Figure 1. Typical two-dimensional ripples. (a, b) – top view in laboratory tank (a) [Voropayev *et al.*, 1999] and in the ocean (b) (this photograph was taken by one of the co-authors at Puerto Peñasco coast, Mexico, October 16 2004 soon after the tide receded); in both cases the ripple length is 6-8 cm; (c, d) – side view of asymmetric ripples in laboratory tank under shoaling waves, (c) - general view, (d) – ripple profile as obtained using the structural light technique; experimental parameters: $\omega = 0.2$ Hz, $\varepsilon_0 = 10$ cm, section # 27 (see below).

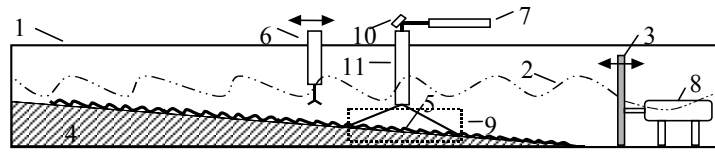


Figure 2. Experimental schematic: 1 – tank, 2 – shoaling water waves, 3 – wave paddle, 4 – sandy slope, 5 – sand ripples, 6 – ADV probe, 7 – laser, 8 – hydraulic system, 9 – view frame of a digital camera which is connected to a computer, 10 – mirror, 11 – light guide with splitting optics.

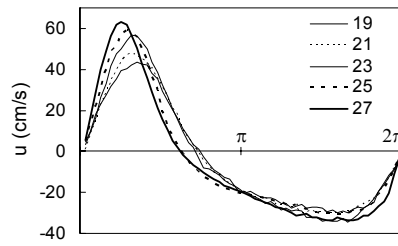


Figure 3. Typical horizontal velocity, u , as measured at the distance 10 cm from the bottom by using an acoustic Doppler velocimeter (ADV). The data were taken in different sections along the slope (shown in the legend) and phase averaged over 40 wave periods. Experimental parameters: $\omega = 0.4$ Hz, $2\varepsilon_0 = 25$ cm.

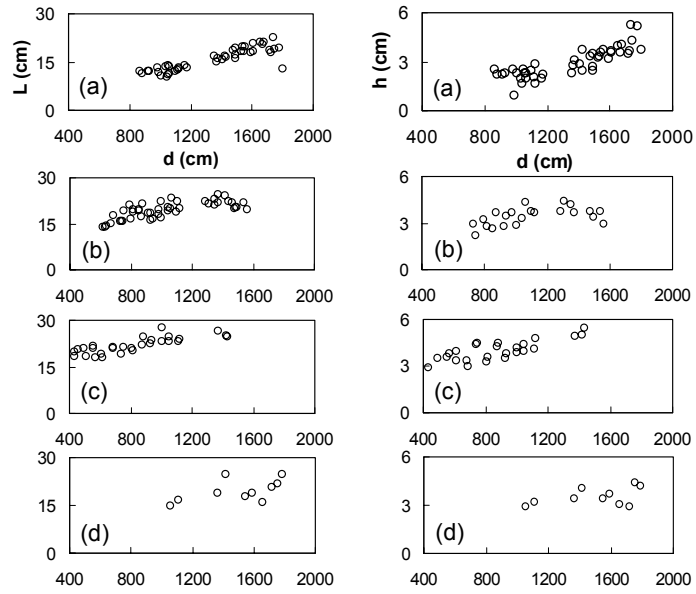


Figure 4. Equilibrium ripple length, L (left column), and height, h (right column), as functions of distance, d , along the slope for 4 different runs. Experimental parameters: (a) - $\omega = 0.4$ Hz, $2\varepsilon_0 = 15$ cm, (b) - 0.4, 20, (c) - 0.4, 25, (d) - 0.2, 20.

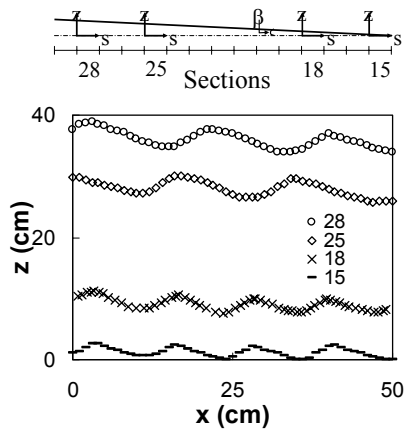


Figure 5. Typical sand surface elevations for different sections (given in the legend) along the slope. To show the profiles taken at different sections in one graph, we use s coordinate to indicate the horizontal distance from the onshore side of each section, and the initial sand level at the offshore side of section 15 was chosen as the origin for the z coordinate (see schematic at the top of the figure). Experimental parameters: $\omega = 0.4$ Hz, $2\varepsilon_0 = 15$ cm.

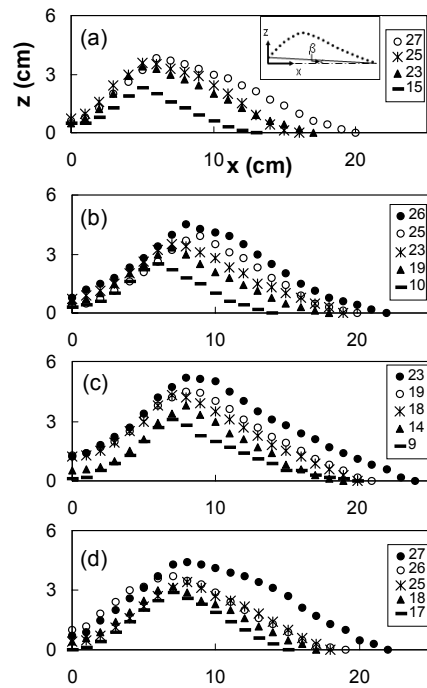


Figure 6. Typical equilibrium ripple profiles taken at different sections along the slope in four different experimental runs. Section numbers are given in legends. The insert in (a) explains the coordinate system.. Experimental parameters: (a) - $\omega = 0.4$ Hz, $2\epsilon_0 = 15$ cm, (b) - 0.4, 20, (c) - 0.4, 25 and (d) - 0.2, 20.

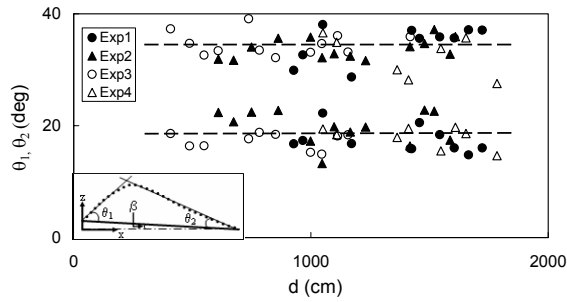


Figure 7. Onshore, θ_1 , and offshore, θ_2 , angles of the ripples as measured along the slope for different experimental runs. A “saw tooth” shape profile and coordinate system are shown in the inset. Different symbols correspond to different experimental runs (given in the legend). Symbols near the upper (lower) dashed line represent the data for θ_1 (θ_2) whereas the dashed lines give the best fit to these data. Experimental parameters: $\omega = 0.4$ Hz, $2\varepsilon_0 = 15$ cm (Exp 1); 0.4, 20 (Exp 2); 0.4, 25 (Exp 3) and 0.2, 20 (Exp 4).

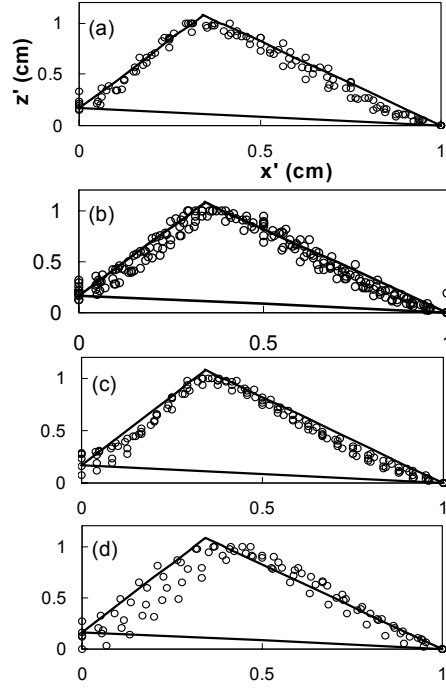


Figure 8. Dimensionless ripple profiles as measured at different sections along the slope for different experimental runs. Symbols – measurements, solid lines – approximation (1). Total of 30 ripple profiles [7 in (a), 12 (b), 6 (c), 5 (d)] are shown. Experimental parameters: $\omega = 0.4$ Hz, $2\varepsilon_0 = 15$ cm (a); 0.4, 20 (b); 0.4, 25 (c), 0.2, 20 (d).